

Research Paper

Improved PET Imaging of uPAR Expression Using new ⁶⁴Cu-labeled Cross-Bridged Peptide Ligands: Comparative *in vitro* and *in vivo* Studies

Morten Persson^{1,2,3,4}, Masood Hosseini^{1,5}, Jacob Madsen⁴, Thomas J. D. Jørgensen⁶, Knud J Jensen^{1,5}, Andreas Kjaer^{1,3,4}, Michael Ploug^{1,2,✉}

1. The Danish-Chinese Center for Proteases and Cancer;
2. Finsen Laboratory, Rigshospitalet & BRIC, Copenhagen Biocenter, Denmark;
3. Cluster for Molecular Imaging, Faculty of Health Sciences, University of Copenhagen, Copenhagen, Denmark;
4. Department of Clinical Physiology, Nuclear Medicine and PET, Center for Diagnostic Investigations, Rigshospitalet, Copenhagen, Denmark;
5. Department of Chemistry, University of Copenhagen, Denmark;
6. Department of Biochemistry and Molecular Biology, University of Southern Denmark, Denmark.

✉ Corresponding author: Michael Ploug, PhD, Dr.Sci. Finsen Laboratory & BRIC, Copenhagen Biocenter, Ole Maaløes Vej 5, 2200 – Copenhagen N, Denmark. E-mail: m-ploug@finsenlab.dk Tel: +45-35456037.

© Ivyspring International Publisher. This is an open-access article distributed under the terms of the Creative Commons License (<http://creativecommons.org/licenses/by-nc-nd/3.0/>). Reproduction is permitted for personal, noncommercial use, provided that the article is in whole, unmodified, and properly cited.

Received: 2013.05.31; Accepted: 2013.07.21; Published: 2013.08.03

Abstract

The correlation between uPAR expression, cancer cell invasion and metastases is now well-established and has prompted the development of a number of uPAR PET imaging agents, which could potentially identify cancer patients with invasive and metastatic lesions. In the present study, we synthesized and characterized two new cross-bridged ⁶⁴Cu-labeled peptide conjugates for PET imaging of uPAR and performed a head-to-head comparison with the corresponding and more conventionally used DOTA conjugate. Based on in-source laser-induced reduction of chelated Cu(II) to Cu(I), we now demonstrate the following ranking with respect to the chemical inertness of their complexed Cu ions: DOTA-AE105 << CB-TE2A-AE105 < CB-TE2A-PA-AE105, which is correlated to their corresponding demetallation rate. No penalty in the uPAR receptor binding affinity of the targeting peptide was encountered by conjugation to either of the macrobicyclic chelators (IC₅₀ ~ 5-10 nM) and high yields and radiochemical purities (>95%) were achieved in all cases by incubation at 95°C. *In vivo*, they display identical tumor uptake after 1h, but differ significantly after 22 hrs, where the DOTA-AE105 uptake remains surprisingly high. Importantly, the more stable of the new uPAR PET tracers, ⁶⁴Cu-CB-TE2A-PA-AE105, exhibits a significantly reduced liver uptake compared to ⁶⁴Cu-DOTA-AE105 as well as ⁶⁴Cu-CB-TE2A-AE105, (p<0.0001), emphasizing that our new *in vitro* stability measurements by mass spectrometry predicts *in vivo* stability in mice. Specificity of the best performing ligand, ⁶⁴Cu-CB-TE2A-PA-AE105 was finally confirmed *in vivo* using a non-binding ⁶⁴Cu-labeled peptide as control (⁶⁴Cu-CB-TE2A-PA-AE105^{mut}). This control PET-tracer revealed significantly reduced tumor uptake (p<0.0001), but identical hepatic uptake compared to its active counterpart (⁶⁴Cu-CB-TE2A-PA-AE105) after 1h. In conclusion, our new approach using in-source laser-induced reduction of Cu(II)-chelated PET-ligands provides useful information, which are predictive for the tracer stability *in vivo* in mice. Furthermore, the increased stability of our new macrobicyclic ⁶⁴Cu-CB-TE2A-PA-AE105 PET ligand is paralleled by an excellent imaging contrast during non-invasive PET scanning of uPAR expression in preclinical mouse cancer models. The translational promises displayed by this PET-tracer for future clinical cancer patient management remains, however, to be investigated.

Key words: urokinase-type plasminogen activator receptor, CD87, positron emission tomography, biomarker, CB-TE2A, Ly-6, SPR, tumor targeting.

Introduction

Development of novel PET ligands for cancer diagnosis and therapy monitoring has accelerated considerably during the last decade, reflecting the steadily growing knowledge on molecular drivers and biomarkers of pathogenesis in several human cancer diseases [1]. One receptor found to correlate to cancer pathogenesis due to its ability to modulate extracellular matrix degradation, which is considered to impact tumor invasion and metastasis, is the urokinase-type plasminogen activator receptor (uPAR) [2, 3]. This high-affinity receptor for uPA is tethered to the cell surface via a glycosyl-phosphatidylinositol (GPI) membrane anchor [4]. Besides facilitating focal plasminogen activation by receptor-bound urokinase-type plasminogen (uPA) [5], increasing evidence also implicates uPAR in cell adhesion and migration by modulating various cell signaling pathways [6]. Levels of shed forms of uPAR in blood furthermore predict poor prognosis in various cancer types such as breast, lung, prostate and colorectal cancer [7]. Since uPAR is implicated in the remodeling of the extracellular matrix during cancer invasion, it is considered to be a relevant anti-cancer target [5, 8], and various cytotoxic intervention strategies targeting uPAR have accordingly been developed, including "intelligent" pro-drugs requiring proteolytic activation by receptor-bound uPA [9], radiotherapeutics [10, 11], and uPAR-mediated internalization of functionalized nanoparticles [12, 13, 14]. Another virtue from a therapeutic perspective is the assumption that uPAR is readily druggable due to its protein architecture with a large hydrophobic uPA-binding cavity [15], its accessibility on the cell surface, and the mild overt phenotypes associated with its genetic ablation [16, 17]. Importantly, its expression levels in solid tumors are also considered an important biomarker for poor prognosis in various human cancers [7] rendering it an obvious candidate for non-invasive biomarker targeted PET imaging in the assessment of cancer patients with aggressive disease [5].

We have previously developed and characterized ^{64}Cu - [18,19], ^{68}Ga - [20], and ^{18}F -labelled [21] peptide PET probes for non-invasive imaging of uPAR expressing in tumor bearing animals based on the macrocyclic chelators DOTA, NODAGA, and NOTA conjugated to a high-affinity 9-mer linear peptide (denoted AE105), which specifically targets human uPAR [22] *i.e.* ^{64}Cu -DOTA-AE105 [23], ^{68}Ga -DOTA/NODAGA-AE105 [24], and ^{18}F -AIF-NOTA-AE105. Initially, we obtained very promising results using ^{64}Cu -DOTA-AE105, where a high tumor-to-background was found and a signifi-

cant correlation between tumor uptake values and levels of uPAR expression were noted, thus validating the *in vivo* specificity of this particular PET probe [19]. However, the use of DOTA as a general chelator for ^{64}Cu has been challenged in a number of studies, where its relatively low kinetic stability allegedly enables a significant transchelation and/or transmetalation of ^{64}Cu *in vivo* to superoxide dismutase and metallothionein in liver as well as albumin in the blood circulation. This suboptimal chelation-chemistry consequently causes an elevated non-specific uptake in these compartments [25, 26]. In line with these limitations, we also noted a relatively high uptake in both liver and blood in tumor bearing mice using ^{64}Cu -DOTA in our studies [18, 19].

This inherent *in vivo* instability of the ^{64}Cu -DOTA complex has prompted an extensive search for improved radionuclide metal chelators with higher *in vitro* and *in vivo* stability [27]. First, 1,4,8,11-tetraazacyclotetradecane-1,4,8,11-tetraacetic acid (TETA) demonstrated higher *in vivo* stability compared to DOTA, but its baseline ^{64}Cu dissociation still resulted in binding to superoxide dismutase *in vivo* [28]. Second, introduction of several tetra-amine based macrobicyclic chelators, in which an ethylene bridge connects two nonadjacent nitrogens, significantly improve their *in vivo* stability compared to the monocyclic DOTA and TETA [29-32]. In particular, the use of CB-TE2A as chelator for ^{64}Cu has been used with success in a number of *in vivo* studies for PET imaging of integrins [33, 34], somatostatin receptor subtype 2 (SSTR2) [35, 36], epidermal growth factor receptor (EGFR) [37] and gastrin-releasing peptide receptor (GRPr) [38, 39], where superior tumor-to-background ratios were reported in all cases compared to the DOTA counterparts. Recently, a CB-TE2A analogue with a propionamide functionalized linker (CB-TE2A-PA) was developed by Boswell et al. [40] (Figure 1). The virtue of this macrobicyclic chelator is that it engages all six coordination sites of Cu^{2+} thus forming an uncharged Cu complex in the final peptide conjugated PET probe, in contrast to the positively charged and five coordinated complex using the original CB-TE2A.

The aims of the present study are to perform the first head-to-head *in vitro* and *in vivo* evaluation of the two cross-bridge cyclam chelators CB-TE2A and CB-TE2A-PA, conjugated to AE105 for uPAR PET imaging, and to compare the tumor-to-background ratios with the DOTA-conjugate analogue *in vivo* in mice carrying human U87MG glioblastoma xenotransplants.

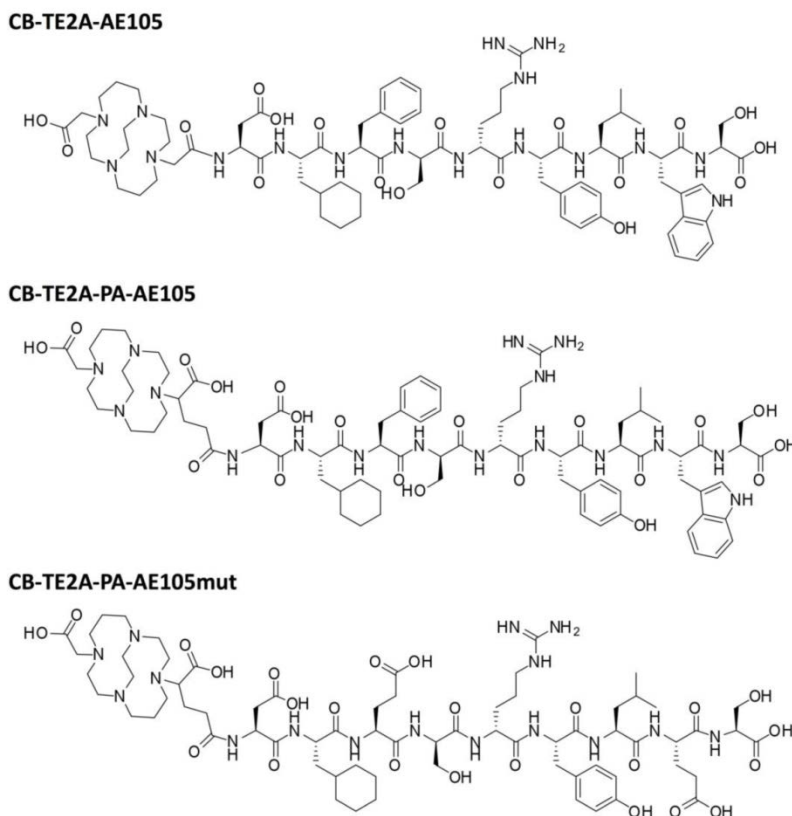


Fig 1. Chemical structures of the uPAR targeting ligands: CB-TE2A-AE105, CB-TE2A-PA-AE105 and inactive control peptide CB-TE2A-PA-AE105^{mut}, where Phe→Glu and Trp→Glu replacements grossly impairs the AE105-uPAR binding interface defined by the corresponding X-ray crystal structure [15].

Materials and methods

Chemical reagents

All commercial chemicals were of analytic grade and were purchased from Sigma-Aldrich, CheMatech, Fluka, Iris Biotech GmbH, or Rapp Polymere GmbH, and used without further purification unless otherwise stated. NMR was performed using a Bruker Advance 300 spectrometer and matrix assisted laser desorption mass spectrometry (MALDI-MS) was performed on a Bruker autoflex II TOF/TOF (Bruker Daltonics, Germany). Analytical HPLC was performed on a Dionex UltiMate 3000, using a Phenomenex Gemini 110 Å C18 column (3 μm, 4.6 × 50 mm) with a flow rate of 1.0 mL/min and a 10 minutes linear gradient going from 95% H₂O/5% acetonitrile with 0.1% HCOOH to 100% acetonitrile 0.1% HCOOH. Preparative HPLC was performed on a Dionex UltiMate 3000, equipped with a Phenomenex Gemini-NX C18 110 Å column operated at a flow rate of 10.0 mL/min and a 30 minutes linear gradient from 95% H₂O/5% acetonitrile with 0.1% TFA to 100% acetonitrile with 0.1% TFA. 2-(4,7,10-tris(2-*tert*-butoxy-2-oxoethyl)-1,4,7,10-tetraazacyclo-dodecan-1-yl)-acetic acid (DOTA-tris(tBu) ester) was purchased from

CheMatech (Dijon, France). ⁶⁴CuCl₂ in 0.1 M HCl was obtained from Risø (DTU, Denmark). Recombinant human uPAR and pro-uPA were expressed in *Drosophila* S2-cells and purified as described [41, 42].

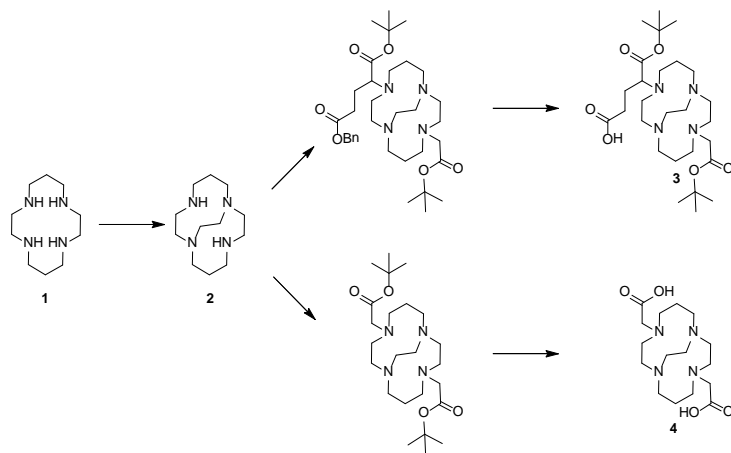
General methods for solid-phase peptide synthesis

Peptide synthesis was performed using N^α-Fmoc protected amino acids and HBTU/HOBt activation using a polystyrene resin with 2-Cl-Trityl linker (0.61 mmol/g) or Tentagel resin with a trityl linker (0.20 mmol/g). HBTU (3.7 equiv.) HOBt/HOAt (4:1, 4 equiv.), Fmoc-AA-OH (4 equiv.), DIEA (7.2 equiv.) in *N*-methyl-2-pyrrolidone (NMP) were used. Preactivation (5 min) and couplings (90 min). Fmoc deprotection was performed by two incubations (15 min each) in piperidine/NMP (1:4). Following peptide assembly and coupling to the respective macrocyclic chelator, the resin was washed extensively with NMP and CH₂Cl₂, before the conjugates were released by 2 hours incubation with TFA/H₂O/triethylsilane (95:2.5:2.5). The released peptide was subsequently collected by filtration and pooled with the two washes with TFA used to clean the resin. This TFA-peptide mixture was stirred at room temperature for 24 hours

before TFA was removed under a stream of nitrogen and the peptide was precipitated with diethyl ether. The synthesized peptides were dissolved in a minimum amount of H₂O/acetonitrile (2:1) before being purified by preparative HPLC and lyophilized.

Synthesis of cross-bridged macrobicyclic chelators

Compound 2: 1,4,8,11-tetraazabicyclo[6.6.2]hexadecane (CB-Cyclam) [29, 43].



In brief; a solution of 5.5 g 1,4,8,11-tetraazacyclotetradecane (27.5 mmol) [cyclam **1**] in 100 mL EtOH was added to 5.5 mL glyoxal (40 % in H₂O) and the mixture was left stirring for 16 h. The mixture was evaporated and re-dissolved in 150 mL acetonitrile. To this solution was added 25 mL benzyl bromide and 300 mg tetrabutylammonium iodide (1.8 mmol). The mixture was stirred for 40 h before the *N,N'*-dibenzylated product was precipitated from the reaction mixture and collected by filtration (10 g, 90%).

A fraction of this precipitate (2.1 g, 5.1 mmol) was dissolved in 50 mL EtOH, added 400 mg NaBH₄ (10.5 mmol), stirred at room temperature until the reaction was complete according to LCMS (1 h), and finally quenched by adding 5 mL NH₄Cl (aq.), and left stirring overnight. After addition of 100 mL saturated NaHCO₃ (aq.), the aqueous phase was extracted with 3 x 100 mL CH₂Cl₂. The product was isolated by evaporation (2.1 g), dissolved in 20 mL AcOH and 5 % (w/w) Pd/C, degassed (Ar), connected to hydrogen balloon, and stirred overnight (16 h). The spent catalyst was removed by filtration, the volatile solvent was evaporated, and the remaining solid redissolved in 20 mL H₂O. The pH of the solution was adjusted to 14 by solid NaOH, extracted with 6 x 25 mL benzene, and the organic phase was finally dried (NaSO₄) and evaporated under reduced pressure to produce a clear

yellow oil (550 mg, 47%). NMR was in accordance with previous published data [31].

Compound 3: 5-(*tert*-butoxy)-4-(11-(2-(*tert*-butoxy)-2-oxoethyl)-1,4,8,11-tetraazabicyclo[6.6.2]hexadecan-4-yl)-5-oxopentanoic acid (protected CB-TE2A-PA). A solution of 800 mg CB-Cyclam (3.53 mmol) [compound **2**] in 200 mL acetonitrile received 2 g K₂CO₃ and 1325 mg (3.71 mmol) α -bromoglutaric acid-1-*tert*-butylester-5-benzyl ester (in 4 portions over 24 h). 790 mg (4.05 mmol) *tert*-butyl bromoacetate was subsequently added to this suspension, left stirring at room temperature (4 h) before being acidified with AcOH and concentrated by evaporation. The benzyl group was removed by hydrogenation (THF, Pd/C, 4 bar, 18 h), the catalyst removed by filtration, and the mixture purified by HPLC yielding 1022 mg [compound **3**] (55%).

Compound 4: 4,11-bis(carboxymethyl)-1,4,8,11-tetraazabicyclo[6.6.2]hexadecane (CB-TE2A). To a solution of 500 mg CB-Cyclam (2.21 mmol) [**2**] in 100 mL acetonitrile were added 1.5 g K₂CO₃ and 900 mg (4.66 mmol) *tert*-butyl bromoacetate. The mixture was stirred 24 h at room temperature, acidified with AcOH, concentrated by evaporation, and finally purified by HPLC. Yield 382 mg, 38%. The *tert*-butyl

groups were removed prior to use to generate [compound **4**] by treatment with TFA at room temperature for 6 hours (important for complete removal).

Synthesis of uPAR-targeting peptides with N-terminal macrocyclic chelators

The uPAR-targeting core peptide AE105 (Asp-Cha-Phe-(D)Ser-(D)Arg-Tyr-Leu-Trp-Ser) and a corresponding inactive variant AE105^{mut} (Asp-Cha-Glu-(D)Ser-(D)Arg-Tyr-Leu-Glu-Ser) were synthesized using *N* α -Fmoc protected amino acids and a polystyrene resin with 2-Cl-Trityl linker (0.61 mmol/g). These peptides (0.1 mmol) were conjugated *in situ* on the resin by adding either 137 mg *tert*-butyl protected CB-TE2A (0.40 mmol) or 211 mg CB-TE2A-PA (0.40 mmol), which were pre-activated with 137 mg *N*[(1*H*-benzotriazol-1-yl)(dimethylamino)methylene]-*N*-methylmethanaminium hexafluorophosphate-*N*-oxide (0.36 mmol) and 0.12 mL *N,N*-diisopropylethylamine (0.72 mmol) in 2 mL *N*-methyl-2-pyrrolidinone. The mixture was shaken for 2 hours, the peptide conjugates released with TFA/H₂O/triethylsilane (95:2.5:2.5), and purified by preparative HPLC using a Phenomenex Gemini-NX C18 110 Å column running at a flow rate of 10 mL/min and a 30 minutes linear gradient from 95% H₂O/5% acetonitrile with 0.1% TFA to 100% acetonitrile with 0.1% TFA. Yields of the purified peptides were: CB-TE2A-AE105 (10 mg; MH⁺: 1550.74 Da/ Δ m

0.09 Da), CB-TE2A-AE105^{mut} (24 mg; MH⁺: 1547.81 Da/ Δ m 0.08 Da), CB-TE2A-PA-AE105 (16 mg; MH⁺: 1622.91 Da/ Δ m 0.06 Da), CB-TE2A-PA-AE105^{mut} (4 mg; MH⁺: 1547.81 Da/ Δ m 0.04 Da). DOTA-AE105 was synthesized as previously described [19].

Radiochemistry

Radiolabeling of all uPAR-targeting peptides conjugated to various macrocyclic chelators (DOTA, CB-TE2A and CB-TE2A-PA) (Figure 1) with ⁶⁴Cu were done by adding 2 nmol conjugated peptide to a vial containing 500 μ L sodium acetate buffer (0.5 M, pH 8) and 50 μ L (approx. 100 MBq) ⁶⁴CuCl₂ in 0.1 M HCl. The solution was heated to 95°C for 30 min. After completion of the synthesis a small aliquot was retrieved for analysis using RP-HPLC as previously described [19]. The reaction mixture was then passed through a C18 SepPak cartridge and free Cu²⁺ was eluted with 5 mL water. The radiolabeled peptide was finally eluted with 0.5 mL ethanol and diluted in water to reduce the ethanol concentration below 5% before tail vein injection. The radiochemical purity of the final product was determined by RP-HPLC. This protocol typically yielded 95 MBq of radiolabeled peptide with a radiochemical purity of 95-97%. The amount of unlabeled Cu²⁺ was less than 1% in the final product.

Potency and specificity of the targeting constructs

To assess the penalty on the uPAR-binding affinity of AE105 by conjugation of CB-TE2A or CB-TE2A-PA to its α -amino-group, the inhibitory effect (IC₅₀) of 3-fold dilution series the corresponding conjugates on the interaction between immobilized pro-uPA and 0.5 nM uPAR were assessed by surface plasmon resonance and compared to that of the unmodified AE105. These studies were enabled by choosing running conditions that confer strict mass transport limitations on the binding reaction between pro-uPA and uPAR, as outlined previously in detail [44]. The direct binding between immobilized uPAR^{wt} (28 fmol/mm²) and 2-fold dilution series of the various targeting constructs were also measured by surface plasmon resonance using a Biacore T200 operated at 20°C and a flow rate of 50 μ L/min running buffer (*i.e.* 10 mM HEPES, 150 mM NaCl, 3 mM EDTA, and 0.1 % (v/v) surfactant P-20 at pH 7.4). Regeneration of the CM5 sensor chip was accomplished by two consecutive 20 μ L injections of 1 M formic acid. Kinetic rate constants (k_{on} and k_{off}) were derived by fitting the double referenced data to a 1:1 binding model using the evaluation software supplied with the instrument.

Cell line and animal model

U87MG glioblastoma cancer cells expressing high levels of uPAR expression [18, 19] were obtained from the American Type Culture Collection (Manassas, VA, USA) and culture media was obtained from Invitrogen Co. (Carlsbad, CA, USA). The cell line was cultured in DMEM supplemented with 10% (v/v) fetal bovine serum and 1% (v/v) penicillin/streptomycin at 37°C and 5% CO₂. Xenografts of human U87MG glioblastoma cancer cells was established by injection of 200 μ L cells (1 \times 10⁸ cells/mL) suspended in 100 μ L Matrigel (BD Biosciences, San Jose, CA, USA), subcutaneously into the left and right flank of female NMRI nude mice obtained from Taconic, under anesthesia by Fentanyl (Hypnorm®) / Midazolam (Doricum®). All animal experiments were performed under a protocol approved by the Animal Research Committee of the Danish Ministry of Justice.

MicroPET/CT Imaging

Ten minutes static PET scans were acquired on a small animal PET Focus 120 scanner (Siemens Medical Solutions, Malvern, PA) 1 and 22 hrs post *i.v.* injection of approximately 10 MBq radiolabeled peptide. PET/CT scanning conditions were all set as described previously [19]. Results were analyzed using Inveon software (Siemens Medical Solutions) and PET data was expressed as percent of injected dose per gram tissue (%ID/g) based on manual region-of-interest drawing on fused PET-CT images for better anatomical localization of organs/tissues of interest.

Biodistribution studies

Biodistribution studies were performed as described [19]. In brief, Nude mice bearing U87MG xenografts received 2-3 MBq of radiolabeled peptide by tail-vein injections. All mice were euthanized after 1 or 22 hrs post tracer injection. Blood, tumor and major organs were collected (wet-weight) and the radioactivity was measured using a γ -counter from Perkin Elmer, MA, USA (n=4 mice/group).

uPAR ELISA

Levels of uPAR in resected U87MG tumors lysates were determined by a validated ELISA as described [19] with one minor improvement. In the present study, we used a mechanical tissue homogenization (Precellys, Bertin Technologies) to pulverize the resected and frozen tumor xenograft as compared to the manual homogenization used previously. All data measurements were performed in duplicates.

Statistical analysis

All quantitative data are expressed as means \pm SEM (standard error of the mean) and means are

compared using one-way ANOVA. P values ≤ 0.05 were considered statistically significant.

Results

Impact on uPAR-targeting affinity by chemical conjugation to various macrocyclic chelators

In the present study, we synthesized and purified two new PET derivatives of a 9-mer linear peptide AE105 [22], which targets human uPAR with high affinity and specificity *in vivo*, by conjugating it to different macrobicyclic chelators using its NH₂-terminus (Figure 1). Our synthesis protocol yielded mg quantities of pure products. The impact on uPAR binding by conjugating AE105 to these macrocyclic chelators was subsequently tested by employing two different assay platforms based on surface plasmon resonance. In the first array of analyses, we measured the inhibitory effect (IC₅₀-values) of these peptides in solution on the binding of 0.5 nM uPAR to immobilized pro-uPA. Under such equilibrium binding conditions, we observed no significant differences in the inhibitory potencies of the various AE105 conjugates yielding IC₅₀-values between 5.9

and 6.7 nM (Figures 2A, 2B, and Table 1). No inhibition was observed for the corresponding control peptides at the highest concentrations tested (600 nM). In the second array of analyses, we measured the direct binding of the conjugated peptides to immobilized uPAR on the sensor chip to obtain the kinetic rate constants for these interactions. In general, neither k_{on} nor k_{off} differs profoundly between the different AE105 derivatives giving rise to K_D-values in the lower nanomolar range, which is in excellent agreement with the recorded IC₅₀-values (Table 1). Nevertheless, CB-TE2A-PA-AE105 did present a slightly weaker binding to immobilized uPAR (K_D 27 nM) as compared to the other derivatives (K_D 8-12 nM) indicating that the more bulky propionamid linker in this conjugate may introduce a moderate imperfection of the uPAR•AE105 interface. Importantly, none of the control peptides revealed any specific interaction with immobilized uPAR in this direct binding assay. Representative real-time binding profiles for these kinetic analyses are shown in Figures 2C and 2D for CB-TE2A-PA-AE105 and its corresponding non-binding CB-TE2A-PA-AE105^{mut}.

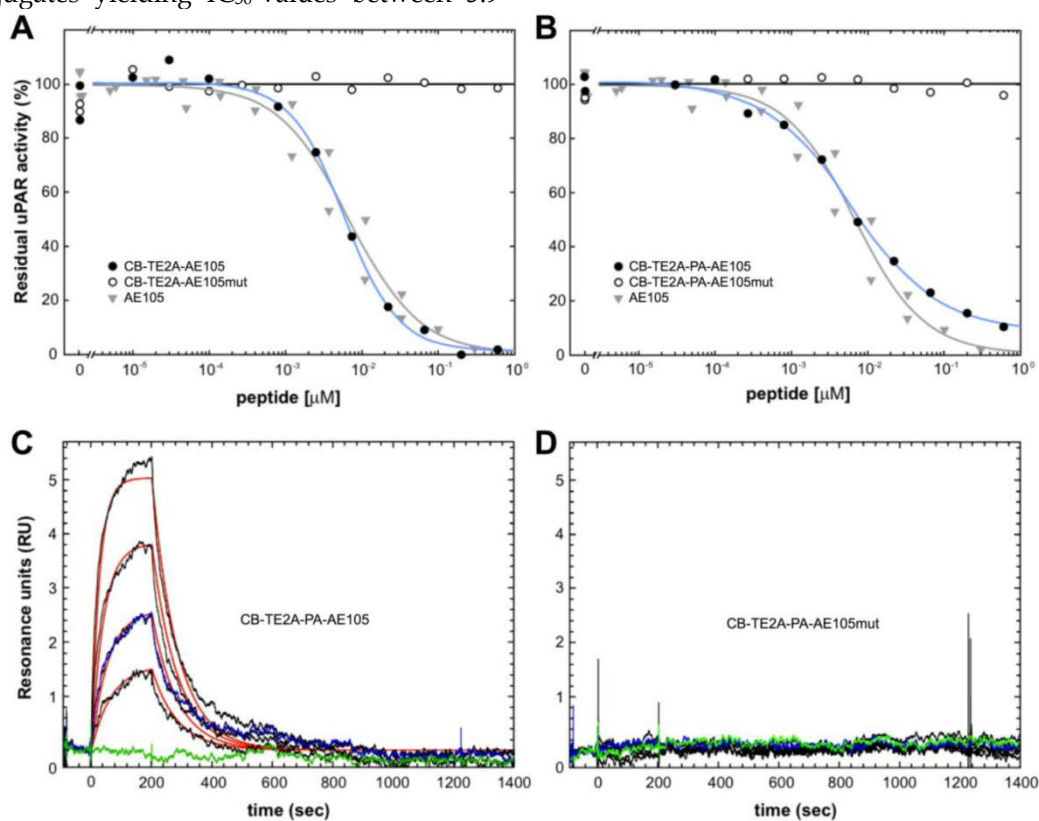


Fig 2. Binding properties of uPAR-targeting PET probes using surface plasmon resonance. The inhibitory profiles of CB-TE2A-AE105 and CB-TE2A-PA-AE105 and their corresponding inactive control peptides are shown in panels A and B, respectively. In these experiments the binding of 0.5 nM recombinant uPAR to immobilized pro-uPA (4300 RU \sim 93 fmol/mm²) are recorded under conditions conferring severe mass transport limitations. The amount of residual, unoccupied uPAR was calculated from the linear association rates in the initial phases of the binding reaction. The IC₅₀-values were calculated by fitting the data to a four-parameter logistic model. The kinetics of the interaction between immobilized uPAR and a 2-fold dilution series of CB-TE2A-AE105 and its corresponding inactive control is shown in panels C and D, respectively. Highest concentration of the peptide tested is 100 nM and 25 nM is measured twice to validate reproducibility. Repeat measurements are shown in blue and buffer runs in green.

Table 1. Binding properties of selected uPAR targeting peptide-based PET probes^a

Ligand	k_{on} ($10^6 M^{-1} s^{-1}$)	k_{off} ($10^{-3} s^{-1}$)	K_D ($10^{-9} M$)	IC_{50} ($10^{-9} M$)
AE105	0.62 ± 0.34	7.6 ± 0.7	12	6.7 ± 1.6
DOTA-AE105	0.46 ± 0.19	4.3 ± 0.6	9.4	6.7 ± 1.0
DOTA-AE105 ^{mut}	nb ^b	nb ^b	nb ^b	>> 10 ³
CB-TE2A-AE105	0.60 ± 0.30	4.6 ± 0.1	7.7	5.9 ± 1.0
CB-TE2A-AE105 ^{mut}	nb ^b	nb ^b	nb ^b	>> 10 ³
CB-TE2A-PA-AE105	0.40 ± 0.13	10.8 ± 0.1	27	6.1 ± 1.0
CB-TE2A-PA-AE105 ^{mut}	nb ^b	nb ^b	nb ^b	>> 10 ³

^aThe IC_{50} -values for competing the binding between 0.5 nM uPAR^{wt} and immobilized pro-uPA were determined as outlined in Figures 2A and 2B. Kinetic rate constants (k_{on} and k_{off}) for the direct interaction with immobilized uPAR^{wt} were determined by surface plasmon resonance using a Biacore T200 as illustrated for CB-TE2A-PA-AE105 and its inactive version in Figure 2C and 2D. The equilibrium dissociation constant (K_D) was calculated as k_{off}/k_{on} . ^bnb: no measurable binding up to 200 nM peptide.

In vitro stability of Cu-complexes of the various uPAR-targeting peptides

Our three purified, active uPAR-targeting peptides DOTA-AE105, CB-TE2A-AE105 and CB-TE2A-PA-AE105 were subsequently loaded with the natural occurring isotopes of Cu(II) (69.2 % ⁶³Cu and 30.8 % ⁶⁵Cu) by incubating them with 10 mM CuCl₂ for 60 minutes at 70°C and the complexes were subsequently purified by RP-HPLC (data not shown). The pure complex preparations were analyzed by MALDI-MS after co-crystallization with α -cyano-4-hydroxycinnamic acid (ACHA) or sinapinic acid (SA) using identical laser pulse energies and delayed extraction times (130 ns) for recording the MS spectra (shown in Figure 3). Despite our pure peptide-complex preparations are stable as judged after repeat RP-HPLC chromatography, the MALDI-MS spectra recorded in ACHA, nevertheless, clearly reveals the occurrence of a variable amount of demetallated peptide with the following ranking according to stability: CB-TE2A-PA-AE105 (19 %) > CB-TE2A-AE105 (36 %) >> DOTA-AE105 (57 %), where the observed loss of Cu induced by laser desorption from ACHA are shown in brackets (Figure 3B to 3D and Table 2). The difference between the monoisotopic masses of the demetallated species and the corresponding Cu-complexes is 60.9 Da in both matrices for all three constructs corresponding to the mass of ⁶³Cu²⁺ minus two protons. The isotope envelopes recorded for the three Cu-complexes are, nonetheless, very different and simulations of the isotope

distributions (Figure 3, left) estimate the abundances of complexed Cu(II) to be markedly diminished for ⁶³Cu-DOTA-AE105 (17 %) compared to both ⁶³Cu-CB-TE2A-AE105 (65 %) and ⁶³Cu-CB-TE2A-PA-AE105 (75 %). The molecular basis for this instability of the complexes during the matrix-assisted desorption process is presumably an in-source decay, where gas phase collisions in the electron dense MALDI plume during delayed extraction cause a reduction of Cu(II) to Cu(I) by electron transfer [45-47]. The reduction of complexed Cu(II) to Cu(I) by gas phase electron transfer during the MALDI process depends on the recombination energy of Cu(II), which is correlated to the thermodynamic probability of electron uptake. Particularly relevant to our present study is the observation, that high affinity binding to Cu(II) lowers its recombination energy, which accordingly renders Cu(II) tethered to strong chelating groups less prone to electron uptake [47]. Our experimental data in Fig. 3 clearly show, that reduction of Cu(II) to Cu(I) occurs much more readily when bound to DOTA as compared to the two macrobicyclic chelators and we ascribe this higher reactivity to a higher recombination energy, which in turn reflects an attenuated gas-phase binding affinity. In this respect, it should be emphasized that the binding energy of Cu(II) generally is much higher compared to Cu(I), which is illustrated by the differences in the total binding energies between Cu(I) and Cu(II) to three imidazoles in the gas phase (625 kJ/mol and 2000 kJ/mol, respectively [47]). In summary, we envision that reduction of Cu(II) to Cu(I) in the MALDI process substantially weakens the interaction between the copper ion and the macrocyclic chelator and this drives the loss of copper (demetallation) via the Cu(I)-peptide complexes during the internal energy build-up in the MALDI plume. Sinapinic acid is a "softer" matrix yielding ions with lower internal energy and the extent of demetallation of Cu(I)-peptide complexes is thus lower for this matrix. From these experiments it is evident that both our cross-bridged macrobicyclic chelators are by far more resilient towards reduction mediated demetallation than DOTA, with CB-TE2A-PA-AE105 showing the best performance (Figure 3 and Table 2).

⁶⁴Cu radiolabeling of ligands

The radiochemical yield obtained for all three uPAR-targeting ligands were >95% using 2 nmol peptid-conjugate and 30 min total reaction time (95°C, pH 8). Using lower amounts of peptide-conjugate significantly reduced the overall yields, with less than 10% yield using 0.5 nmol CB-TE2A-AE105 (Figure 4). The radiolabeled peptides were purified on a Sep-Pak

C18 cartridge to remove unbound ^{64}Cu , which resulted in > 95% pure products. The specific activities

of the final radiolabeled conjugates were all approximately 50 GBq/ μmol .

Table 2. Laser-induced in-source reduction of Cu(II) complexed to various macrocyclic chelators.

Ligand - matrix ¹	Demetallation (%) ²	$^{63}\text{Cu(II)}/^{63}\text{Cu}$ (%) ³	Isotope control (%) ⁴
DOTA-AE105			
CHCA	57.1 ± 8.0	15.3 ± 5.2	50.9 ± 0.4
SA	18.1 ± 6.9	41.1 ± 4.9	51.1 ± 1.2
CB-TE2A-AE105			
CHCA	36.2 ± 7.8	44.8 ± 3.1	52.2 ± 1.6
SA	23.2 ± 3.3	46.0 ± 2.1	51.3 ± 0.9
CB-TE2A-PA-AE105			
CHCA	19.2 ± 2.9	45.6 ± 1.4	51.0 ± 0.9
SA	4.4 ± 1.2	46.6 ± 1.5	50.0 ± 3.5

¹The following MALDI matrices were used in this study α -cyano-4-hydroxycinnamic acid (CHCA) and sinapinic acid (SA). ²Estimation of the degree of in-source prompt dissociation of Cu from the macrocyclic chelators. The relative areas of the isotope envelopes representing the demetallated peptide (M) and the Cu-complexed peptide (M+Cu) were calculated for each matrix: $[M/(M+(M+Cu))]\times 100$. The data are shown for 8 independent sample depositions in CHCA and SA. ³Surrogate marker for the degree of laser-induced Cu(II) to Cu(I) reduction that still persists in the Cu-complexes leaving the source of the mass spectrometer. The relative peak heights corresponding to $^{63}\text{Cu(II)}/^{63}\text{Cu}$ were calculated for both matrices (n=8) as $[b/(b+(b+1))]\times 100$ in Figure 3. ⁴Quality control for the above surrogate marker assessment of Cu(II) reduction. The relative peak heights corresponding to the demetallated peptides were measure for both matrices in the same MALDI spectra as $[a/(a+(a+1))]\times 100$ in Figure 3 (n=8).

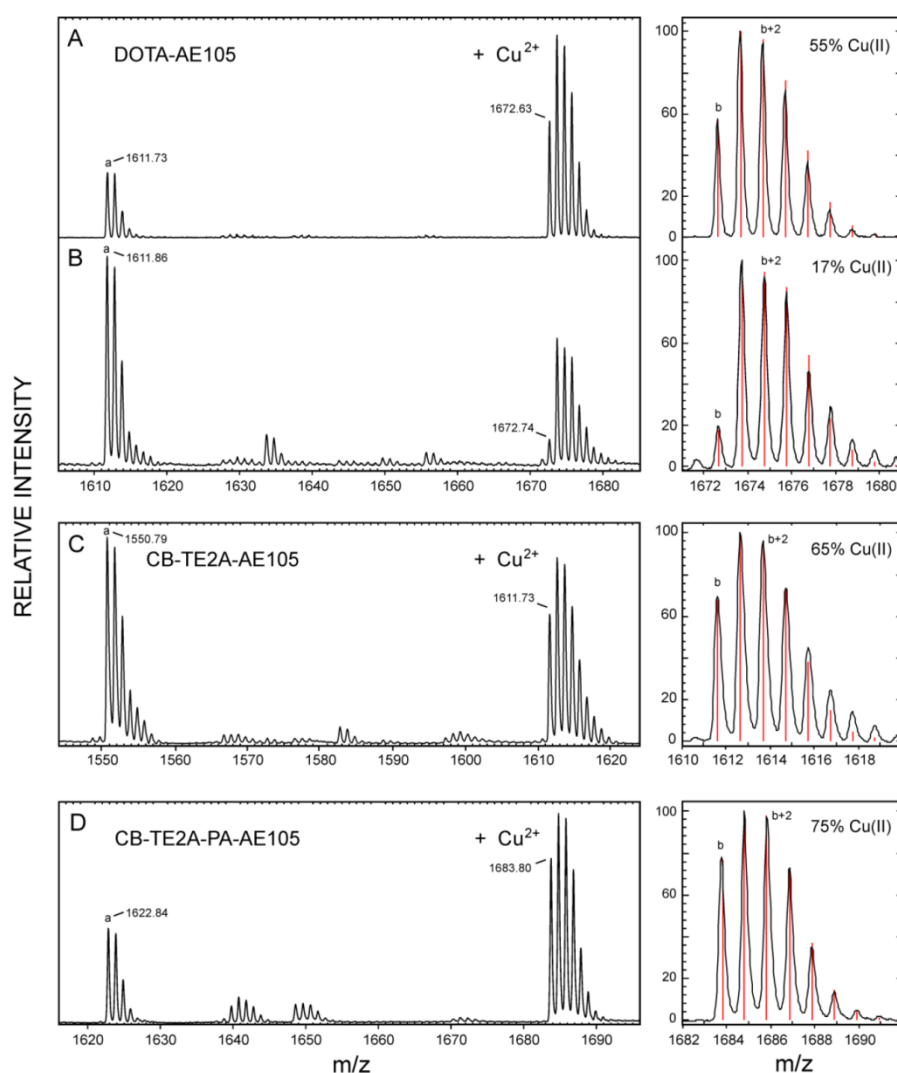


Fig 3. Chemical stability of different macrocyclic Cu-complexes probed by MALDI-MS. MALDI-MS spectra are recorded under identical conditions for Cu-DOTA-AE105 in SA (panel A) and CHCA (panel B), Cu-CB-TE2A-AE105 in CHCA (panel C), and for Cu-CB-TE2A-PA-AE105 in CHCA (panel D). To the left of each panel is shown the best fit obtained for the isotope envelopes using the oxidation state of the bound Cu as the only floating parameter (Cu(II) or Cu(I)). The lower case letters in the MALDI-MS spectra indicates the monoisotopic peaks of the following singly charged molecular species: a) corresponds to the demetallated peptide, $[M + H]^+$; b) corresponds to the Cu-chelated peptide with $^{63}\text{Cu(II)}$, $[M - H + ^{63}\text{Cu(II)}]^+$.

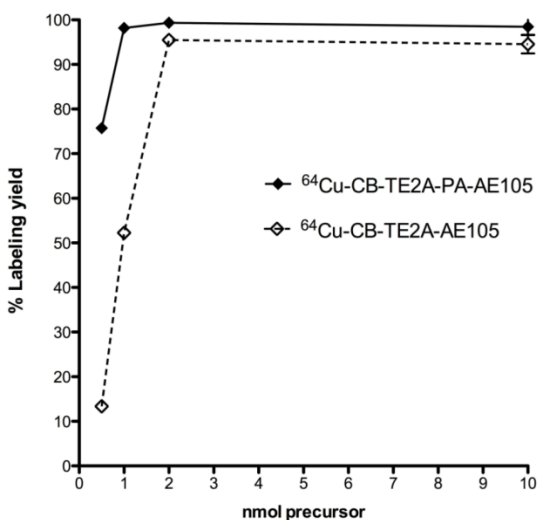


Fig 4. Radiolabeling uPAR targeting peptides. Radiochemical yields for ⁶⁴Cu labeling using different amounts of CB-TE2A-AE105 and CB-TE2A-PA-AE105 incubated 30 min at 95°C and pH 8.0. Above 2 nmol conjugated peptide, no significantly difference in labeling yield were observed, whereas CB-TE2A-PA-AE105 gave a higher yield below 2 nmols.

Head-to-head *in vivo* PET comparison

In the first experiment, a head-to-head *in vivo* PET imaging study of ⁶⁴Cu-DOTA-AE105, ⁶⁴Cu-CB-TE2A-AE105 and ⁶⁴Cu-CB-TE2A-PA-AE105 for uPAR PET imaging was performed in parallel on a cohort of nude mice inoculated at the same time with human U87MG tumor cells. Such xenografts generally express high levels of uPAR [19]. All three ligands showed a high tumor uptake, with ⁶⁴Cu-CB-TE2A-AE105, ⁶⁴Cu-CB-TE2A-PA-AE105, and ⁶⁴Cu-DOTA-AE105 having uptake values of 3.5±0.8 %ID/g, 4.2±0.6 %ID/g and 4.8±0.7 %ID/g, respectively (Figure 5A) providing a good contrast for imaging tumor localization by PET scanning already after 1h *p.i.* (Figure 5E). After 22 hrs the relative tumor uptake values declined as expected for the two macrobicyclic derivatives to 2.0±0.3 %ID/g and 1.6±0.3 %ID/g, whereas the DOTA-based probe remained unaltered at 4.5±2.2 %ID/g.

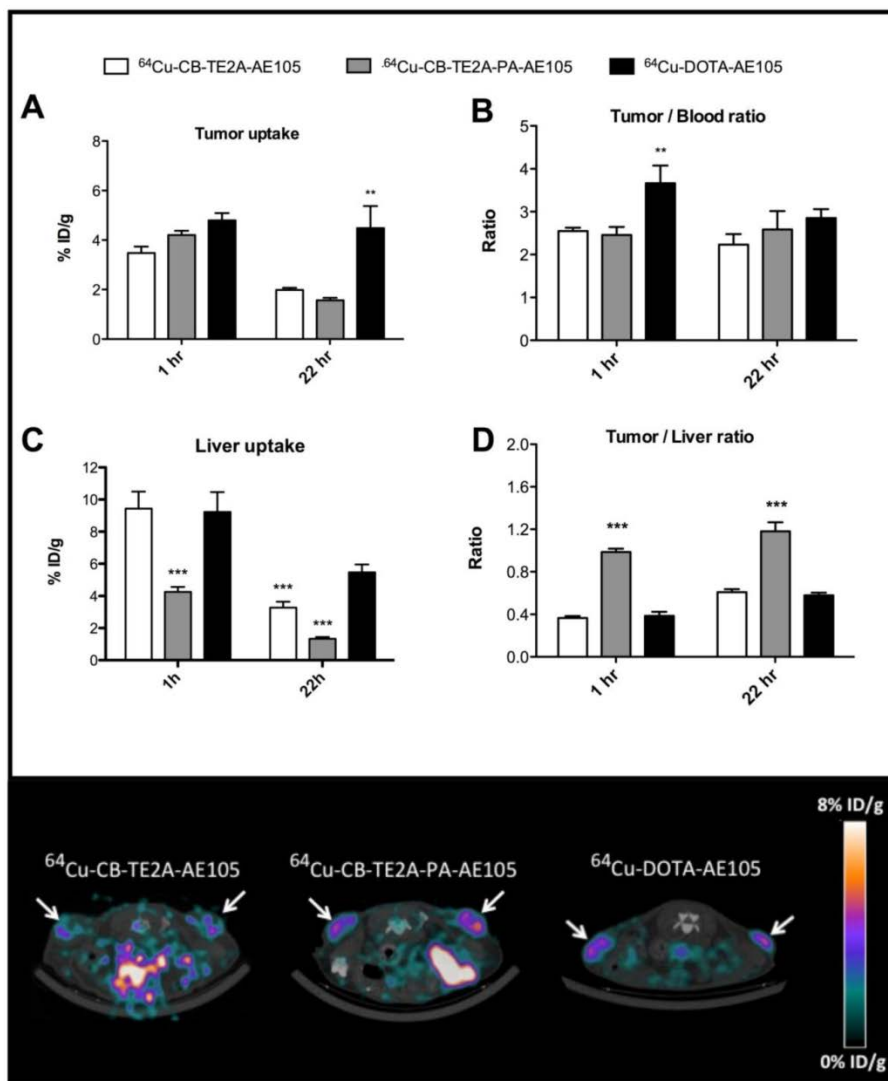


Fig 5. Quantitative ROI analysis from PET imaging of all three uPAR ligands. Tumor uptake values (%ID/g) after 1 hr and 22 hrs are shown in panel A, tumor-to-blood ratio in panel B, liver uptake values in panel C, and tumor-to-liver ratio in panel D. Representative transverse images of ⁶⁴Cu-DOTA-AE105 and ⁶⁴Cu-CB-TE2A-AE105 are shown in the lower panel for 1 h *p.i.* White arrow indicates tumor. ** p<0.01, *** p<0.001. (n=8 tumors).

As reported previously by others [26, 34, 38], we also observed a significant difference in the hepatic uptake value for ^{64}Cu -CB-TE2A-AE105 as compared to ^{64}Cu -DOTA-AE105 at 22hrs ($p < 0.001$). This reduced hepatic uptake was, however, even more pronounced for ^{64}Cu -CB-TE2A-PA-AE105 (Figure 5C) indicating that this particular PET tracer exhibits the better *in vivo* stability of the three tested uPAR ligands. Unexpectedly, no significant differences in tumor-to-liver ratios were found in this study between ^{64}Cu -DOTA-AE105 and ^{64}Cu -CB-TE2A-AE105 after either 1h (0.39 ± 0.10 and 0.37 ± 0.06) or 22hrs (0.58 ± 0.06 and 0.61 ± 0.09), respectively (Figure 5D). In contrast, a significantly improved tumor-to-liver ratio was importantly found for ^{64}Cu -CB-TE2A-PA-AE105 (1h: 0.99 ± 0.10 , $p < 0.001$ and 22hrs: 1.18 ± 0.27 , $p < 0.001$) compared to both ^{64}Cu -DOTA-AE105 and ^{64}Cu -CB-TE2A-AE105. ^{64}Cu -DOTA-AE105 presents a significantly higher tumor-to-blood ratio (3.66 ± 1.09 , $p < 0.01$) compared to ^{64}Cu -CB-TE2A-AE105 (2.55 ± 0.25) and ^{64}Cu -CB-TE2A-PA-AE105 (2.46 ± 0.59) 1h *p.i.* (Figure 5B), but this difference is not retained in images recorded after 22 hrs.

Biodistribution

Biodistribution studies were performed in nude mice bearing uPAR-positive U87MG xenografts. ^{64}Cu -CB-TE2A-AE105 and ^{64}Cu -CB-TE2A-PA-AE105 were administered by a single *i.v.* injection and organs and tissue were collected after 1h and 22 hrs *p.i.* Figures 6A and 6B show the radionuclide uptake after 1h and 22 hrs, respectively. Both ligands cleared rapidly from the blood (< 2.0 %ID/g after 1 h). Kidney uptake decreased more slowly, with approximate 14 %ID/g after 1 h and 5% ID/g at 22 hrs *p.i.* Overall, a very similar general uptake was observed for each of the ligands, although ^{64}Cu -CB-TE2A-PA-AE105 has a tendency to clear faster from non-target tissues.

A 2-fold increase in hepatic uptake was consistently observed after 1 h and 22 hrs for ^{64}Cu -CB-TE2A-AE105 (1 h: 11.2 ± 1.2 %ID/g, 22 hrs: 3.6 ± 0.4 %ID/g) compared to ^{64}Cu -CB-TE2A-PA-AE105 (1 h: 4.8 ± 0.2 %ID/g, 22 hrs: 1.6 ± 0.1 %ID/g). Importantly, this property improves the tumor-to-liver ratio significantly for ^{64}Cu -CB-TE2A-PA-AE105 (1 h: $p < 0.01$ and 22 hrs: $p < 0.001$, Figure 6C), which is excellently aligned with the previous PET scanning profiles recorded for a similar experiment (Fig. 5E) thus validating the improved *in vivo* partitioning of this particular uPAR-targeting PET tracer. All data from the biodistribution study are shown in Table 3.

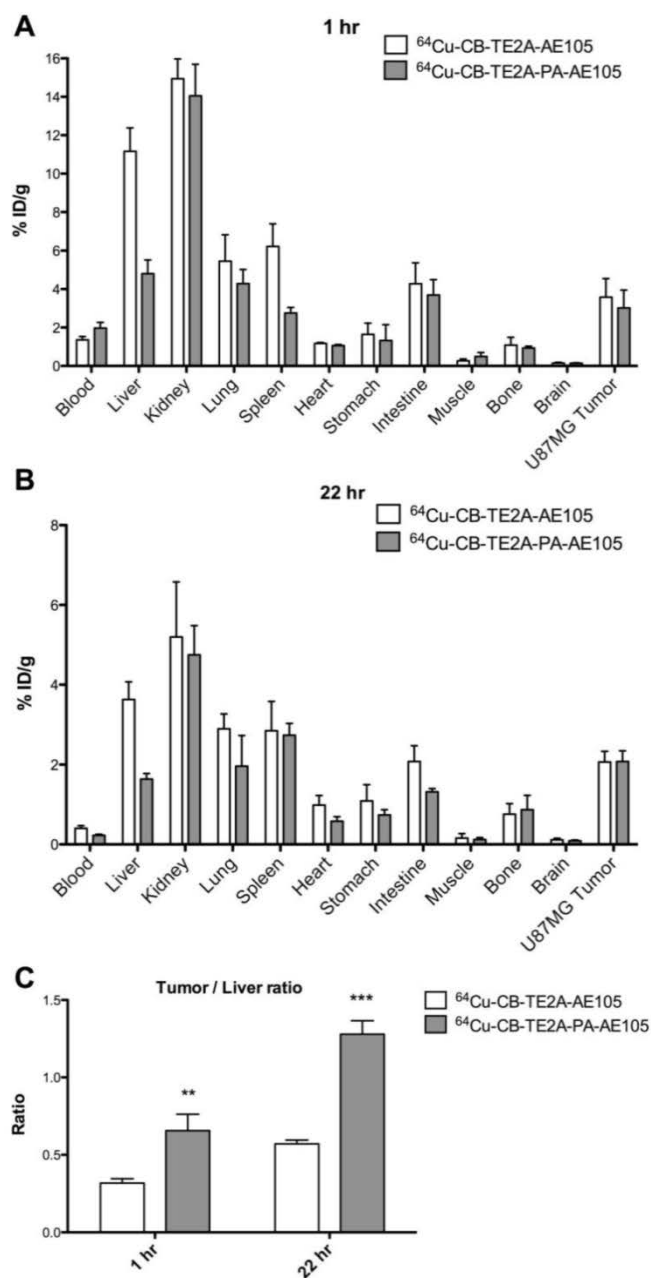


Fig 6. Biodistribution profiles of uPAR PET tracers. Results for ^{64}Cu -CB-TE2A-AE105 and ^{64}Cu -CB-TE2A-PA-AE105 are shown after 1 h (panel A) and 22 hrs (panel B). A significantly higher tumor-to-liver ratio was found for ^{64}Cu -CB-TE2A-PA-AE105 after both 1h ($p > 0.01$) and 22 h ($p > 0.001$) (panel C). ($n = 4$ mice/group).

Table 3. Biodistributions of new cross-bridged uPAR PET tracers^a.

Organ	⁶⁴ Cu-CB-TE2A-AE105		⁶⁴ Cu-CB-TE2A-PA-AE105	
	1 h (%ID/g)	22 hrs (%ID/g)	1 h (%ID/g)	22 hrs (%ID/g)
Blood	1.4 ± 0.2	0.4 ± 0.1	2.0 ± 0.3	0.2 ± 0.1
Liver	11.2 ± 1.2	3.6 ± 0.4	4.8 ± 0.7	1.6 ± 0.1
Kidney	15.0 ± 1.0	5.2 ± 1.4	14.0 ± 1.6	4.8 ± 0.7
Lung	5.5 ± 1.4	2.9 ± 0.4	4.3 ± 0.7	2.0 ± 0.8
Spleen	6.2 ± 1.2	2.9 ± 0.7	2.8 ± 0.3	2.7 ± 0.3
Heart	1.2 ± 0.1	1.0 ± 0.2	1.1 ± 0.1	0.6 ± 0.1
Stomach	1.7 ± 0.6	1.1 ± 0.4	1.3 ± 0.8	0.7 ± 0.1
Intestine	4.3 ± 1.1	2.1 ± 0.4	3.7 ± 0.8	1.3 ± 0.1
Muscle	0.3 ± 0.1	0.2 ± 0.1	0.5 ± 0.2	0.1 ± 0.1
Bone	1.1 ± 0.4	0.8 ± 0.3	0.9 ± 0.1	0.9 ± 0.3
Brain	0.2 ± 0.1	0.1 ± 0.1	0.1 ± 0.1	0.1 ± 0.1
Tumor	3.6 ± 1.0	2.1 ± 0.3	3.0 ± 0.9	2.0 ± 0.3
Tumor-to-nontumor ratios				
Tumor-to-blood	2.6 ± 0.5	5.2 ± 0.5	1.5 ± 0.4	9.3 ± 1.7
Tumor-to-liver	0.3 ± 0.1	0.6 ± 0.1	0.7 ± 0.3	1.3 ± 0.2
Tumor-to-kidney	0.2 ± 0.1	0.4 ± 0.1	0.2 ± 0.1	0.5 ± 0.1
Tumor-to-intestine	0.8 ± 0.1	1.0 ± 0.2	0.9 ± 0.3	1.6 ± 0.2
Tumor-to-muscle	1.4 ± 0.2	17.5 ± 8.0	7.5 ± 5.0	22.2 ± 15.3

^aThe biodistributions profiles and tumor to non-tumor ratios for ⁶⁴Cu-CB-TE2A-AE105 and ⁶⁴Cu-CB-TE2A-PA-AE105 were established in nude mice bearing U87MG xenografts by gamma counting of resected organs.

In vivo specificity study

To demonstrate that the tumor uptake of the best performing PET-tracer (*i.e.* ⁶⁴Cu-CB-TE2A-PA-AE105) is indeed caused by a specific targeting of uPAR rather than passive accumulation of free ⁶⁴Cu²⁺, we measured the *in vivo* uptake by PET scanning of a non-binding version of our targeting probe labeled with ⁶⁴Cu to the same specific activity. The successful abrogation of the targeting affinity of the designed control peptide towards uPAR was confirmed by surface plasmon resonance studies revealing the IC₅₀ to be reduced from 5-10 nM to >> 1 μM for the dysfunctional peptide and no direct binding can accordingly be measured (Figure 2 and Table 1). When parallel PET/CT images of this control PET probe were reconstructed for 1 h and compared to the corresponding active uPAR-targeting probe, a significantly reduced tumor uptake was found (*p*<0.001, Figure 7B). This effect is clearly visualized by the reconstructed PET images (Figure 7A). The tumor uptake value was 5.4±0.7 %ID/g for ⁶⁴Cu-CB-TE2A-PA-AE105 after 1 h. In contrast, the tumor uptake value in mice injected in parallel with the non-binding version ⁶⁴Cu-CB-TE2A-PA-AE105^{mut} having the same specific radioactivity was only 2.2±0.4 %ID/g after 1 h. Importantly, the hepatic uptake values of these active and inactive PET-tracers were comparable after 1 h (Figure 7B). Noteworthy, the hepatic uptake val-

ues (representing a non-target organ) were significantly lower for the ⁶⁴Cu-CB-TE2A-PA-AE105 PET-tracer compared to both ⁶⁴Cu-DOTA-AE105 and ⁶⁴Cu-CB-TE2A-AE105 (Figure 5C). Moreover, the difference in tumor uptake was clearly not related to differences in uPAR expression between the two groups as ELISA measurements on resected tumors lysates revealed comparable uPAR levels (Figure 7C). Combined these data unambiguously confirms the uPAR-targeting specificity of ⁶⁴Cu-CB-TE2A-PA-AE105.

Discussion

Our present study reports on the synthesis and characterization of two new ⁶⁴Cu labeled cross-bridged peptide antagonists that specifically targets human uPAR. Importantly, our data reveal that the new ⁶⁴Cu-CB-TE2A-PA-AE105 PET-tracer in our experiments exhibits a much improved tumor-to-liver ratio compared to both ⁶⁴Cu-CB-TE2A-AE105 and ⁶⁴Cu-DOTA-AE105, which is in accordance with the *in vitro* stabilities we measured by MALDI-MS.

The rational design of these uPAR-targeting PET-tracers was originally guided by our detailed knowledge on the structure-functional relationships that drive the biochemistry of this receptor - as reviewed recently [48]. Accordingly, we observed no significant impact on the affinity and specificity of the uPAR-targeting core-peptide by conjugation to any of the macrocyclic chelators employed in this study. Nonetheless, in the direct binding assay CB-TE2A-PA-AE105 did present a slightly weaker affinity to immobilized uPAR (K_D 27 nM) as compared to the other derivatives (K_D 8-12 nM) indicating that the propionamid linker in this particular conjugate may introduce a moderate imperfection of the uPAR•AE105 binding interface. Despite this notion, we did not observe a similar difference in the IC₅₀-values for the solution phase competition experiments (Table 1) emphasizing the similar potencies of the various peptide conjugates. The differences observed in the direct binding to the immobilized receptor could therefore pertain to changes in the conformation of the inherently flexible uPAR [49] introduced by the immobilization chemistry, which is sensed only by the more bulky peptide conjugate *i.e.* CB-TE2A-PA-AE105. Importantly, none of the control peptides revealed any specific interaction with immobilized uPAR in this direct binding assay further substantiating their usefulness as reporters of non-specific probe accumulation *in vivo*.

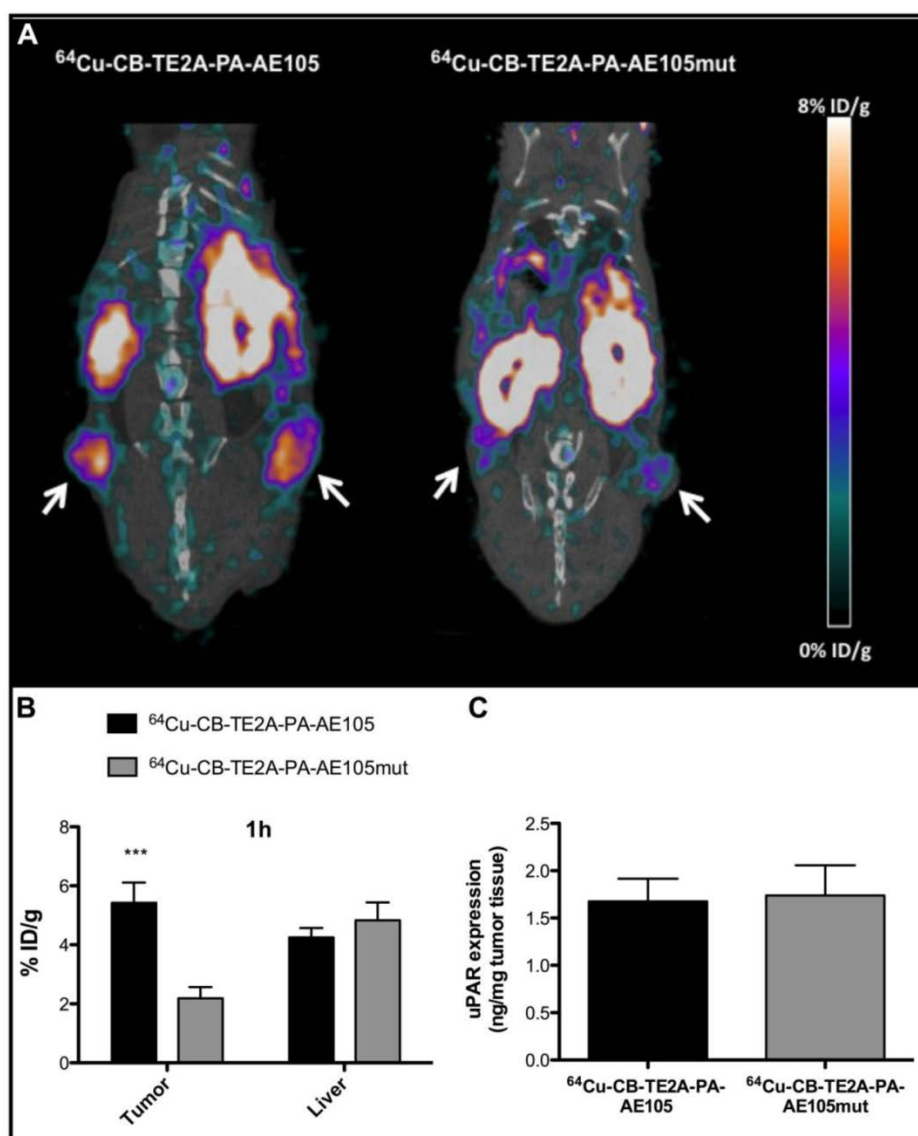


Fig 7. Specificity of uPAR imaging by ^{64}Cu -CB-TE2A-PA-AE105 targeting. Representative sagittal PET/CT images for ^{64}Cu -CB-TE2A-PA-AE105 and its corresponding inactive control peptide ^{64}Cu -CB-TE2A-PA-AE105^{mut} are shown after 1 h (panel A). White arrows indicate location of the tumors. The corresponding quantitative ROI analysis of tumor and liver are shown (panel B). Levels of uPAR expression determined by ELISA in resected tumor lysates from mice sacrificed after termination of each imaging experiment are shown in (panel C). (n = 6 tumors (3 mice in each group)). *** p<0.001.

Radionuclide labeling of these uPAR targeting ligands with $^{64}\text{Cu}^{2+}$ was completed within 30 min at 95°C, pH 8 (yields > 95 %) using as little as 2 nmol conjugated peptide (Figure 4). This reaction kinetic is somewhat faster than those generally reported, where 1 h to 2 hrs of incubation is typically required for completion [40, 50]. However, the relatively harsh radiolabeling conditions still limits radiolabeling to relatively stable peptide conjugates excluding radiolabeling of proteins and antibodies. To overcome these limitations, a second-generation cross-bridge chelators incorporating methanephosphoric acid pendent arms (CB-TE2P and CB-TE1A1P) was recently published [51, 52]. These chelators enable cop-

per radiolabeling at room temperature within 1 h and data shows improved biodistribution compared with CB-TE2A [53]. However, no conjugation to any proteins using these chelators has yet been reported.

The introduction of a propionamide arm in CB-TE2A-PA neutralizes the charge of the resultant copper complex in contrast to the original CB-TE2A chelator [31, 40], where one of the pendant carboxylates is used for conjugation to the peptide. In our present study, we find that this modification does not affect the tumor uptake value, which is comparable to that of the CB-TE2A derivative, but importantly we observe a significantly reduced uptake of the CB-TE2A-PA derivative in non-target organs such as

the liver ($p < 0.001$). Since hepatic accumulation of copper is a valid surrogate marker for compromised *in vivo* stability [26, 53] we propose that CB-TE2A-PA-AE105 possess a superior *in vivo* stability compared to CB-TE2A-AE105. Both our new macrobicyclic PET-tracers targeting uPAR do, nevertheless, exhibit a higher stability than ^{64}Cu -DOTA-AE105 (Figure 5C). In line with this proposition is our new *in vitro* stability data based on MALDI in-plume reduction (Figure 3, Table 2) and a previous report, which states that positively charged ^{64}Cu -labeled cyclam and Et-cyclam chelates generally exhibit a higher liver accumulation compared to the corresponding neutral complex, ^{64}Cu -labeled 3,9-DOC in rats [25].

Somewhat surprisingly, we found no significant differences in the tumor-to-liver ratios between ^{64}Cu -CB-TE2A-AE105 and ^{64}Cu -DOTA-AE105 (figure 5D), despite a significant reduction in the hepatic uptake of ^{64}Cu -CB-TE2A-AE105 at 22 hrs (Figure 5C). The well-established lower kinetic stability of the copper-DOTA complex *in vivo* [25, 26] may, however, represent a major confounding factor in such experiments. The possible contribution from un-bound ^{64}Cu during PET imaging is illustrated by high and persistent tracer accumulations in *e.g.* U87MG xenotransplants after tail vein injection of free $^{64}\text{Cu}^{2+}$; 3.5 ± 0.4 %ID/g and 3.8 ± 0.4 %ID/g at 1 h and 22 hrs, respectively [54]. Accordingly, we speculate that the commonly observed high tumor uptake of ^{64}Cu -DOTA-conjugated ligands in particular, that we and others [51, 52] observe in mice 22 hrs after tracer administration, represents a composite signal from specific receptor targeting as well as non-specific accumulation of free ^{64}Cu in the tumor tissue. A direct comparison of tumor uptake values in mice between ^{64}Cu -labeled DOTA conjugates and new metal chelating systems such as the cross-bridged conjugates used in this study should therefore be interpreted with some precaution due to the different magnitude of confounding effects inherent to tracer leakage *in vivo* from the employed macrocyclic chelators.

At present only very few publications address the *in vivo* use of CB-TE2A-PA. In one study Liu et al [43] synthesize CB-TE2A-PA conjugated to cRGDyK (*i.e.* ^{64}Cu -CB-TE2A-PA-c(RGDyK)) and used this PET-probe for imaging of $\alpha_v\beta_3$ integrin expression in PC3 prostate cancer xenografts *in vivo*, but a parallel comparison to the corresponding CB-TE2A conjugate was regrettably not attempted [43]. Nonetheless, by comparing the reported liver uptake data in mice from Liu et al. [43], (1 h: 1.4 ± 0.1 %ID/g) with the liver uptake data of ^{64}Cu -CB-TE2A-c(RGDyK) published by Anderson et al [55], (1 h: 3.9 ± 2.0 %ID/g) a signifi-

cantly reduced liver uptake (2.8 fold, $p < 0.05$) was indeed seen between the two chelators. Although this may be considered circumstantial evidence, it is intriguing that we find a similar difference in the hepatic uptake in our controlled pairwise comparison of these chelators using a different receptor targeting ligand (2.2 fold, $p < 0.001$).

In conclusion, the present study selects ^{64}Cu -CB-TE2A-PA-AE105 as the most promising peptide tracer for the specific detection of human uPAR expression in xenotransplanted mouse model systems by non-invasive PET imaging among those ^{64}Cu - and ^{68}Ga -labeled derivatives of AE105 that we have tested [18-20]. It should, nevertheless, be emphasized that the confounding effects from the reduced stability of Cu-DOTA complexes that generally affects preclinical imaging in mouse model systems, do not necessarily translate directly to the clinical situation. Accordingly, the use of ^{64}Cu -DOTA-TATE for PET imaging of somatostatin receptor expression in neuroendocrine cancer patients provides very high quality images with a high tumor-to-background contrast and low non-specific hepatic uptake [56]. Selection of the optimal PET tracer for future clinical imaging of uPAR expression in patients is therefore a composite process involving multiple factors and considerations.

Acknowledgments

We thank Gitte Juhl Funch for expert technical assistance and John Post for graphical artwork. This work was supported by The Danish National Research Foundation (Centre for Proteases and Cancer), Danish Medical Research Council, the Danish National Advanced Technology Foundation, the Novo Nordisk Foundation, the Lundbeck Foundation, and the A.P. Moeller Foundation and the Svend Andersen Foundation.

Abbreviations

CB-TE2A: 4,11-*bis*(carboxymethyl)-1,4,8,11-tetraazabicyclo[6.6.2]hexadecane;
 CB-TE2A-PA: 4-carboxymethyl-11-(1,3-dicarboxypropyl)-1,4,8,11-tetraazabicyclo[6.6.2]hexadecane;
 DIEA: *N,N*-diisopropylethylamine;
 DOTA: 1,4,7,10-tetraazacyclododecane-1,4,7,10-tetraacetic acid;
 Fmoc: 9-fluorenylmethyloxycarbonyl;
 HBTU: *N*[(1*H*-benzotriazol-1-yl)(dimethylamino)-methylene]-*N*-methylmethanamonium hexafluorophosphate *N*-oxide;
 HOAt: 3-hydroxy-3*H*-1,2,3-triazolo[4,5-*b*]pyridine or 1-hydroxy-7-azabenzotriazole;
 HOBt: 1-hydroxybenzotriazole;
 PET: positron emission tomography;

uPAR: urokinase-type plasminogen activator receptor.

Competing Interests

The authors have declared that no competing interest exists.

References

- Kramer-Marek G, and Capala J. The role of nuclear medicine in modern therapy of cancer. *Tumour Biol.* 2012; 33: 629-40.
- Rømer J, Nielsen BS, and Ploug M. The urokinase receptor as a potential target in cancer therapy. *Curr. Pharm. Des.* 2004; 10: 2359-76.
- Mekkawy AH, Morris DL, Pourgholami MH. Urokinase plasminogen activator system as a potential target for cancer therapy. *Future Oncol.* 2009; 5: 1487-99.
- Ploug M, Rønne E, Behrendt N, Jensen A L, Blasi F, and Danø K. Cellular receptor for urokinase plasminogen activator. Carboxyl-terminal processing and membrane anchoring by glycosyl-phosphatidylinositol. *J Biol Chem.* 1991; 266: 1926-33.
- Kriegbaum M C, Persson M, Haldager L, Alpizar-Alpizar W, Jacobsen B, Gårdsvoll H, Kjaer A, and Ploug M. Rational targeting of the urokinase receptor (uPAR): development of antagonists and non-invasive imaging probes. *Curr. Drug Targets* 2011; 12: 1711-28.
- Smith H W and Marshall C J. Regulation of cell signalling by uPAR. *Nat. Rev. Mol. Cell. Biol.* 2010; 11: 23-36.
- Rasch MG, Lund IK, Almasi CE and Høyer-Hansen G. Intact and cleaved uPAR forms: diagnostic and prognostic value in cancer. *Front. Biosci.* 2008; 13: 6752-62.
- Mazar AP. Urokinase plasminogen activator receptor choreographs multiple ligand interactions: implications for tumor progression and therapy. *Clin Cancer Res.* 2008; 14: 5649-55
- Su Y, Ortiz J, Liu S, Bugge TH, Singh R, Leppla SH, Frankel AE. Systematic urokinase-activated anthrax toxin therapy produces regressions of subcutaneous human non-small cell lung tumor in athymic nude mice. *Cancer Res.* 2007; 67: 3329-36
- Knör S, Sato S, Huber T, Morgenstern A, Bruchertseifer F, Schmitt M, Kessler H, Senekowitsch-Schmidtke R, Magdolen V, Seidl C. Development and evaluation of peptidic ligands targeting tumour-associated urokinase plasminogen activator receptor (uPAR) for use in alpha-emitter therapy for disseminated ovarian cancer. *Eur J Nucl Med Mol Imaging.* 2008; 35:53-64
- Persson M, Rasmussen P, Madsen J, Ploug M, Kjaer A. New peptide receptor radionuclide therapy of invasive cancer cells: in vivo studies using ¹⁷⁷Lu-DOTA-AE105 targeting uPAR in human colorectal cancer xenografts. *Nucl Med Biol.* 2012; 39:962-9.
- Yang L, Peng XH, Wang YA, Wang X, Cao Z, Ni C, Karna P, Zhang X, Wood WC, Gao X, Nie S, Mao H. Receptor-targeted nanoparticles for in vivo imaging of breast cancer. *Clin Cancer Res.* 2009; 15:4722-32.
- Lee GY, Qian WP, Wang L, Wang YA, Staley CA, Satpathy M, Nie S, Mao H, Yang L. Theranostic nanoparticles with controlled release of gemcitabine for targeted therapy and MRI of pancreatic cancer. *ACS Nano.* 2013; 7:2078-89.
- Hansen L, Unmack Larsen EK, Nielsen EH, Iversen F, Liu Z, Thomsen K, Pedersen M, Skrydstrup T, Nielsen NC, Ploug M, Kjems J. Targeting of peptide conjugated magnetic nanoparticles to urokinase plasminogen activator receptor (uPAR) expressing cells. *Nanoscale.* 2013.
- Llinas P, Le Du M H, Gårdsvoll H, Danø K, Ploug M, Gilquin B, Stura E A, and Ménez A. Crystal structure of the human urokinase plasminogen activator receptor bound to an antagonist peptide. *EMBO J.* 2005; 24: 1655-63.
- Connolly B M, Choi E Y, Gårdsvoll H, Bey AL, Currie BM, Chavakis T, Liu S, Molinolo A, Ploug M, Leppla SH and Bugge TH. Selective abrogation of the uPA-uPAR interaction in vivo reveals a novel role in suppression of fibrin-associated inflammation. *Blood* 2010; 116: 1593-603.
- Ploug M, Plesner T, Rønne E, Ellis V, Høyer-Hansen G, Hansen NE, and Danø K. The receptor for urokinase-type plasminogen activator is deficient on peripheral blood leukocytes in patients with paroxysmal nocturnal hemoglobinuria. *Blood* 1992; 79: 1447-55.
- Li ZB, Niu G, Wang H, He L, Yang L, Ploug M and Chen X. Imaging of urokinase-type plasminogen activator receptor expression using a ⁶⁴Cu-labeled linear peptide antagonist by microPET. *Clin. Cancer Res.* 2008; 14: 4758-66.
- Persson M, Madsen J, Østergaard S, Jensen MM., Jørgensen JT, Juhl K, Lehmann C, Ploug M and Kjaer A. Quantitative PET of human urokinase-type plasminogen activator receptor with ⁶⁴Cu-DOTA-AE105: implications for visualizing cancer invasion. *J. Nucl. Med.* 2012; 53: 138-45.
- Persson M, Madsen J, Østergaard S, Ploug M and Kjaer A. ⁶⁸Ga-labeling and *in vivo* evaluation of a uPAR binding DOTA- and NODAGA-conjugated peptide for PET imaging of invasive cancers. *Nucl. Med. Biol.* 2012; 39: 560-9.
- Persson M, Liu H, Madsen J, Cheng Z, Kjaer A. First ¹⁸F-labeled ligand for PET imaging of uPAR: In vivo studies in human prostate cancer xenografts. *Nucl Med Biol.* 2013; 40: 618-24.
- Ploug M, Østergaard S, Gårdsvoll H, Kovalski K, Holst-Hansen C, Holm A, Ossowski L and Danø K. Peptide-derived antagonists of the urokinase receptor. Affinity maturation by combinatorial chemistry, identification of functional epitopes, and inhibitory effect on cancer cell intravasation. *Biochemistry* 2001; 40: 12157-68.
- [Internet] Leung K. ⁶⁴Cu-1,4,7,10-Tetraazacyclododecane-N,N',N'',N'''-tetraacetic acid-Asp-cyclohexylalanine-Phe-D-Ser-D-Arg-Tyr-Leu-Trp-Ser-NH₂ (AE105-NH₂)⁶⁴Cu-DOTA-AE105-NH₂; Molecular Imaging and Contrast Agent Database (MICAD). <http://www.ncbi.nlm.nih.gov/books/NBK100136/>
- [Internet] Leung K. ⁶⁸Ga-1,4,7-Triazacyclononane,1-glutaric acid-4,7-acetic acid-Asp-cyclohexylalanine-Phe-D-Ser-D-Arg-Tyr-Leu-Trp-Ser-NH₂ (AE105-NH₂) ⁶⁸Ga-NODAGA-AE105-NH₂; Molecular Imaging and Contrast Agent Database (MICAD). <http://www.ncbi.nlm.nih.gov/books/NBK100135/>.
- Jones-Wilson TM, Deal KA, Anderson CJ, McCarthy DW, Kovacs Z, Motekaitis RJ, Sherry AD, Martell AE and Welch MJ. The *in vivo* behavior of copper-64-labeled azamacrocyclic complexes. *Nucl Med Biol.* 1998; 25: 523-30.
- Boswell CA, Sun X, Niu W, Weisman GR, Wong EH, Rheingold AL and Anderson CJ. Comparative *in vivo* stability of copper-64-labeled cross-bridged and conventional tetraazamacrocyclic complexes. *J. Med. Chem.* 2004; 47: 1465-74.
- Anderson CJ, Wadas TJ, Wong EH and Weisman GR. Cross-bridged macrocyclic chelators for stable complexation of copper radionuclides for PET imaging. *Q. J. Nucl. Med. Mol. Imaging* 2008; 52: 185-92.
- Bass LA, Wang M, Welch MJ and Anderson CJ. *In vivo* transchelation of copper-64 from TETA-octreotide to superoxide dismutase in rat liver. *Bioconjug. Chem.* 2000; 11: 527-32.
- Weisman GR, Rogers ME, Wong EH, Jasinski JP and Paight ES. Cross-Bridged Cyclam - Protonation and Li⁺ Complexation in a Diamond-Lattice Cleft. *J. Am. Chem. Soc.* 1990; 112: 8604-8605.
- Weisman GR, Hill DC and Wong EH. Synthesis and transition metal complexes of new cross-bridged tetraamine ligands. *Abstr. Pap. Am. Chem.* 1996; 211: 570.
- Wong EH, Weisman GR, Hill DC, Reed DP, Rogers ME, Condon JS, Fagan MA, Calabrese JC, Lam KC, Guzei IA and Rheingold AL. Synthesis and characterization of cross-bridged cyclams and pendant-armed derivatives and structural studies of their copper(II) complexes. *J. Am. Chem. Soc.* 2000; 122: 10561-10572.
- Sprague JE, Peng Y, Fiamengo AL, Woodin KS, Southwick EA, Weisman GR, Wong EH, Golen JA, Rheingold AL and Anderson CJ. Synthesis, characterization and *in vivo* studies of Cu(II)-64-labeled cross-bridged tetraazamacrocyclic-amide complexes as models of peptide conjugate imaging agents. *J. Med. Chem.* 2007; 50: 2527-2535.
- Zheleznyak A, Wadas TJ, Sherman CD, Wilson JM, Kostenuik PJ, Weilbaecher KN and Anderson CJ. Integrin $\alpha_v\beta_3$ as a PET Imaging Biomarker for Osteoclast Number in Mouse Models of Negative and Positive Osteoclast Regulation. *Mol. Imaging Biol.* 2012; 14: 500-508
- Dumont RA, Deininger F, Haubner R, Maecke HR, Weber WA and Fani M. Novel ⁶⁴Cu- and ⁶⁸Ga-labeled RGD conjugates show improved PET imaging of $\alpha_v\beta_3$ integrin expression and facile radiosynthesis. *J. Nucl. Med.* 2011; 52: 1276-1284.
- Eiblmaier M, Andrews R, Laforest R, Rogers BE and Anderson CJ. Nuclear uptake and dosimetry of ⁶⁴Cu-labeled chelator somatostatin conjugates in an SSTR2-transfected human tumor cell line. *J. Nucl. Med.* 2007; 48: 1390-1396.
- Wadas TJ, Eiblmaier M, Zheleznyak A, Sherman CD, Ferdani R, Liang K, Achilefu S and Anderson CJ. Preparation and biological evaluation of ⁶⁴Cu-CB-TE2A-sst2-ANT, a somatostatin antagonist for PET imaging of somatostatin receptor-positive tumors. *J. Nucl. Med.* 2008; 49: 1819-27.
- Kumar SR, Gallazzi FA, Ferdani R, Anderson CJ, Quinn TP and Deutscher SL. *In vitro* and *in vivo* evaluation of ⁶⁴Cu-radiolabeled KCCYSL peptides for targeting epidermal growth factor receptor-2 in breast carcinomas. *Cancer Biother. Radiopharm.* 2010; 25: 693-703.

38. Garrison JC, Rold TL, Sieckman GL, Figueroa SD, Volkert WA, Jurisson SS and Hoffman TJ. *In vivo* evaluation and small-animal PET/CT of a prostate cancer mouse model using ^{64}Cu bombesin analogs: Side-by-side comparison of the CB-TE2A and DOTA chelation systems. *J. Nucl. Med.* 2007; 48: 1327-1237.
39. Abiraj K, Mansi R, Tamma ML, Fani M, Forrer F, Nicolas G, Cescato R, Reubi JC and Maecke HR. Bombesin antagonist-based radioligands for translational nuclear imaging of gastrin-releasing peptide receptor-positive tumors. *J. Nucl. Med.* 2011; 52: 1970-1978.
40. Boswell CA, Regino CA, Baidoo KE, Wong KJ, Bumb A, Xu H, Milenic DE, Kelley JA, Lai CC and Brechbiel MW. Synthesis of a cross-bridged cyclam derivative for peptide conjugation and ^{64}Cu radiolabeling. *Bioconjug. Chem.* 2008; 19: 1476-1484.
41. Jacobsen B, Gårdsvoll H, Juhl Funch G, Østergaard S, Barkholt V and Ploug M. One-step affinity purification of recombinant urokinase-type plasminogen activator receptor using a synthetic peptide developed by combinatorial chemistry. *Protein Expr. Purif.* 2007; 52: 286-296.
42. Gårdsvoll H, Gilquin B, Le Du MH, Ménez A, Jørgensen TJ and Ploug M. Characterization of the functional epitope on the urokinase receptor. Complete alanine scanning mutagenesis supplemented by chemical cross-linking. *J Biol Chem.* 2006; 281: 19260-19272.
43. Liu W, Hao G, Long MA, Anthony T, Hsieh JT and Sun X. Imparting multivalency to a bifunctional chelator: a scaffold design for targeted PET imaging probes. *Angew. Chem. Int. Ed. Engl.* 2009; 48: 7346-7349.
44. Gårdsvoll H, Jacobsen B, Kriegbaum MC, Behrendt N, Engelholm L, Østergaard S and Ploug M. Conformational regulation of urokinase receptor function: Impact of receptor occupancy and epitope-mapped monoclonal antibodies on lamellipodia induction. *J. Biol. Chem.* 2011; 286: 33544-56.
45. Zhang J, Frankevich V, Knochenmuss R, Friess SD and Zenobi R. Reduction of Cu(II) in matrix-assisted laser desorption/ionization mass spectrometry. *Am. Soc. Mass Spectrom.* 2003; 14: 42-50
46. Knochenmuss R and Zenobi R. MALDI ionization: The role of in-plume processes. *Chem. Rev.* 2003; 103: 441-452
47. Dong J, Vachet RW. Coordination sphere tuning of the electron transfer dissociation behavior of Cu(II)-peptide complexes. *J. Am. Soc. Mass Spectrom.* 2012; 23: 321-9.
48. Ploug, M. Structure-driven design of radionuclide tracers for non-invasive imaging of uPAR and targeted radiotherapy: The tale of a synthetic peptide antagonist. *Theranostics* 2013; 3: 467-76
49. Mertens HD, Kjaergaard M, Mysling S, Gårdsvoll H, Jørgensen TJ, Svergun DI and Ploug M. A flexible multidomain structure drives the function of the urokinase-type plasminogen activator receptor (uPAR). *J. Biol. Chem.* 2012; 287: 34304-34015.
50. Wadas TJ and Anderson CJ. Radiolabeling of TETA- and CB-TE2A-conjugated peptides with copper-64. *Nat. Protoc.* 2006; 1: 3062-3068.
51. Ferdani R, Stigers DJ, Fiamengo AL, Wei L, Li BT, Golen JA, Rheingold AL, Weisman GR, Wong EH and Anderson CJ. Synthesis, Cu(II) complexation, ^{64}Cu -labeling and biological evaluation of cross-bridged cyclam chelators with phosphonate pendant arms. *Dalton Trans* 2012; 41: 1938-1950.
52. Guo Y, Ferdani R and Anderson CJ. Preparation and biological evaluation of ^{64}Cu labeled tyr(3)-octreotate using a phosphonic Acid-based cross-bridged macrocyclic chelator. *Bioconjug. Chem.* 2012; 23: 1470-1477.
53. Sun X, Wuest M, Weisman GR, Wong EH, Reed DP, Boswell CA, Motekaitis R, Martell AE, Welch MJ and Anderson CJ. Radiolabeling and in vivo behavior of copper-64-labeled cross-bridged cyclam ligands. *J. Med. Chem.* 2002; 45: 469-77.
54. Jørgensen JT, Persson M, Madsen J and Kjaer A. High tumor uptake of ^{64}Cu : Implications for molecular imaging of tumor characteristics with copper-based PET tracers. *Nucl. Med. Biol.* 2013; 40: 345-350
55. Wei L, Ye Y, Wadas TJ, Lewis JS, Welch MJ, Achilefu S and Anderson CJ. ^{64}Cu -labeled CB-TE2A and diamsar-conjugated RGD peptide analogs for targeting angiogenesis: comparison of their biological activity. *Nucl. Med. Biol.* 2009; 36: 277-285.
56. Pfeifer A, Knigge U, Mortensen J, Oturai P, Berthelsen AK, Loft A, Binderup T, Rasmussen P, Elema D, Klausen TL, Holm S, von Benzon E, Højgaard L and Kjaer A. Clinical PET of neuroendocrine tumors using ^{64}Cu -DOTATATE: first-in-humans study. *J. Nucl. Med.* 2012; 53: 1207-12015.